Supporting Information

Sharp-Tip Enhanced Catalytic CO Oxidation by Atomically Dispersed Pt_1/Pt_2 on Raised Graphene Oxide Platform

Chuanyi Jia [a, b],‡ Yujin Zhang [c],‡ Xijun Wang [b],‡ Wenhui Zhong [a], Oleg V. Prezhdo [d], Yi Luo [b], Jun Jiang [b,*]

a) Guizhou Provincial Key Laboratory of Computational Nano-material Science, Institute of Applied Physics, Guizhou Education University, Guiyang, Guizhou, 550018, China

b) Hefei National Laboratory for Physical Sciences at the Microscale, iChEM (Collaborative Innovation Center of Chemistry for Energy Materials), CAS Center for Excellence in Nanoscience, School of Chemistry and Materials Science, University of Science and Technology of China, Hefei, Anhui, 230026, China

c) School of Electronic and Information Engineering, Department of Physics, Qilu University of Technology, Jinan, Shandong, 250353, China

d) Department of Chemistry, University of Southern California, Los Angeles, California, 90089, United States

Corresponding Author

* jiangj1@ustc.edu.cn. Phone: +86 551 63600029

‡ The first three authors contributed equally to this work.

1. The Convergence Test for DFT, DFT-D2 and DFT-D3 Calculation Methods.

Three different calculation methods (DFT, DFT-D2 and DFT-D3) have been test, as shown in Table S1. Comparing the value of ***Eb(O_2)***, we noted that using different vdW (van der Waals) corrections (D2 or D3), the ***Eb(O2)*** has very small changes (less than 0.003 eV). However, if we do not use vdW correction (DFT), the changes will become much larger (more than 0.031 eV). The optimized structures in Figure S1 also show that the differences of bond lengths between the DFT and DFT-D2 calculation methods are more significant than the differences between the DFT-D2 and DFT-D3 calculation methods, which further confirm the above conclusion. As a result, the vdW correction is necessary for the two-dimensional system (which is supported by some other DFT calculation works as well[s1,s2]), and a common DFT-D2 method is selected for our calculations.

Table S1. Calculated total energies of bare Pt_1O_2/Gr (***E*(Pt$_1$O$_2$/Gr)**) and O_2+Pt_1O_2/Gr (***E*(O$_2$-Pt$_1$O$_2$/Gr)**), and the binding energies of O_2 (***E*$_b$(O$_2$)**) using different calculation methods.

	DFT	***DFT-D2***	***DFT-D3***
***E*(Pt$_1$O$_2$/Gr)/eV**	-676.284	-680.774	-679.134
***E*(O$_2$-Pt$_1$O$_2$/Gr)/eV**	-688.597	-693.054	-691.417
***E*$_b$(O$_2$)/eV**	-2.456	-2.422	-2.425

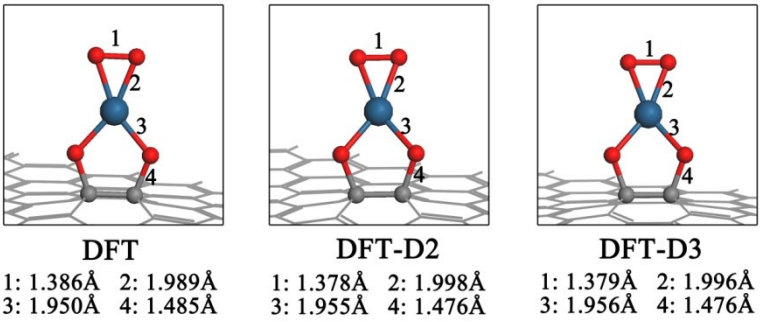

Figure S1. The optimized structures of O_2 on Pt_1O_2/Gr using different calculation methods (DFT, DFT-D2, and DFT-D3). Dark blue, gray, and red spheres represent Pt, C, and O atoms, respectively.

2. The Detailed Calculation Steps for the Reaction Paths.

The calculation steps are as follows (taking the $CO+O_2$ reaction path on Pt_1/Gr as an example): (1) calculate various initial binding states of co-adsorbed $CO+O_2$ on Pt_1/Gr, and select the most stable one (Pt1/Gr-CO-O_2-1), as shown in Figure S2; (2) based on the most stable initial binding states in step (1), design various intermediates/final states; (3) optimize the designed states in step-(2), and select the most stable one; (4) based on the most stable initial binding states and intermediates/final states in step (1) and (3), design various reaction paths (insert different images during CI-NEB calculations); (5) select the most reasonable reaction path and transition state in step (4) to draw the PES (potential energy surface); (6) find the rate limiting step and calculate the energy barrier.

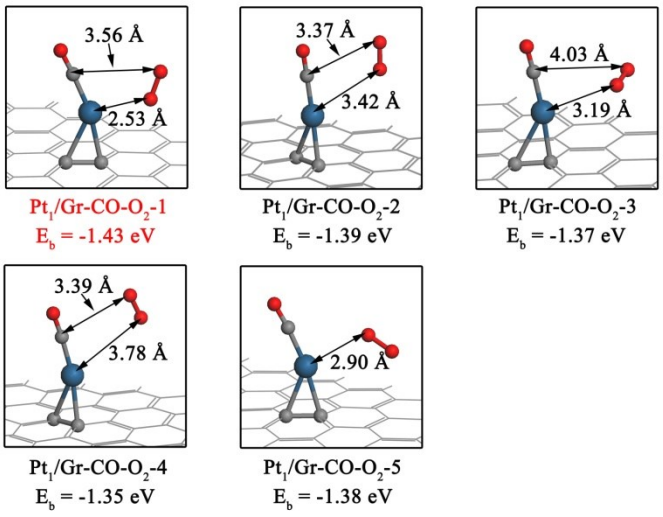

Figure S2. The optimized structures and binding energies of the adsorption states for $CO+O_2$ on Pt_1/Gr. See Figure S1 for color coding.

3. Calculation Details for the Ratio between the Coverage of CO and O_2.

The ratio between the coverage of CO and O_2 is calculated as follows:

The adsorption of CO and O_2 proceeds as [s3]:

$$CO + * \rightarrow CO* \quad \text{(R1)}$$

$$O_2 + * \rightarrow O_2* \quad \text{(R2)}$$

When the reactions R1 and R2 are in equilibrium, the forward and reverse rates are equal:

$$k_1^{+} p(CO)\theta* = k_1^{-}\theta_{CO} \quad (1)$$

$$\theta_{CO} = K_1 p(CO)\theta* \quad (2)$$

$$k_2^{+} p(O_2)\theta* = k_1^{-}\theta_{O_2} \quad (3)$$

$$\theta_{O_2} = K_2 p(O_2)\theta* \quad (4)$$

k_i^{+} and k_i^{-} are the forward and backward rate constants for Ri respectively,

K_i is the rate constant, which is equal to the ratio of k_i^{+} and k_i^{-},

$p(CO)$ and $p(O_2)$ are the partial pressures of CO and O_2: $p(CO)$= 0.01 bar and $p(O_2)$ = 0.21 bar at room temperature,

$\theta*$ represents the coverages of CO and O_2 in terms of free sites.

The coverages of θ_{O_2}, θ_{CO}, and $\theta*$ follow the rule:

$$\theta_{O_2} + \theta_{CO} + \theta* = 1 \quad (5)$$

The rate constant K_1 is given by:

$$K_1 = e^{\frac{-\Delta G_1}{kT}} \quad (6)$$

In this equation, ΔG_1 is the change of Gibb's free energy in R1 which is calculated by [s4]:

$$\Delta G_1 = \Delta E_1 + \Delta ZPE_1 - T\Delta S_1 \quad (7)$$

where, ΔE_1 is the binding energy of CO; ΔZPE_1 is the change in zero-point energy during CO adsorption; T is the temperature (T = 298.15 K), ΔS_1 is the change in entropy during CO adsorption; *k* is the Boltzmann constant.

The rate constant K_2 is given by:

$$K_2 = e^{\frac{-\Delta G_2}{kT}} \quad (8)$$

In this equation, ΔG_2 is the change of Gibb's free energy in R2 which is calculated by:

$$\Delta G_2 = \Delta E_2 + \Delta ZPE_2 - T\Delta S_2 \quad (9)$$

where, ΔE_2 is the binding energy of O_2; ΔZPE_2 is the change in zero-point energy during O_2 adsorption; ΔS_2 is the change in entropy during O_2 adsorption.

Finally, the $\frac{\theta_{CO}}{\theta_{O_2}}$ is calculated as:

$$\frac{\theta_{CO}}{\theta_{O_2}} = \frac{K_1 p(CO)}{K_2 p(O_2)} \quad (10)$$

By evaluating the competition between CO and O_2 in occupying catalytic sites, the ratio $\frac{\theta_{CO}}{\theta_{O_2}}$ is more direct and therefore better in reflecting the CO poisoning effect than the difference in the binding energies/Gibbs free binding energies of CO and O_2. To connect the ratio $\frac{\theta_{CO}}{\theta_{O_2}}$ with the Gibbs free binding energies (for easy comparison), we have also included the Boltzmann constant *k*, temperature *T*, and Napierian logarithm

in eq 2 in the paper. Since Γ_o directly represents the different abilities in capturing CO and O_2 by catalyst, we could name it as "CO poisoning rate".

4. Binding Structures of the Pt_1O_2 Cluster at the Ortho, Meta, and Para Positions of a Carbon Ring on Graphene.

The calculation results show that the Pt_1O_2 cluster can only be adsorbed on the Ortho-position of the ring. When Pt_1O_2 cluster is adsorbed on the Meta and Para positions, it can be easily desorbed and leave far away from the surface, as shown in Figure S1.

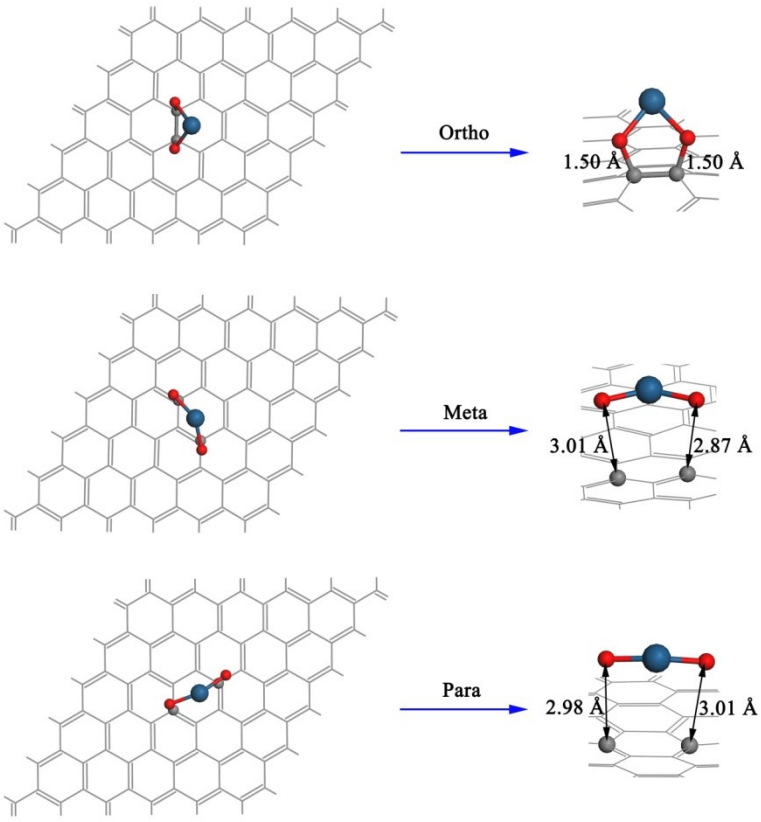

Figure S3. Binding structures of the Pt_1O_2 cluster at the Ortho, Meta, and Para positions of the ring. Left: top-view; Right: side-view. See Figure S1 for color coding.

5. Binding Structures and Corresponding DDEC Charges of the Pt_1/Pt_2-tip on Pristine/Oxidized Graphene.

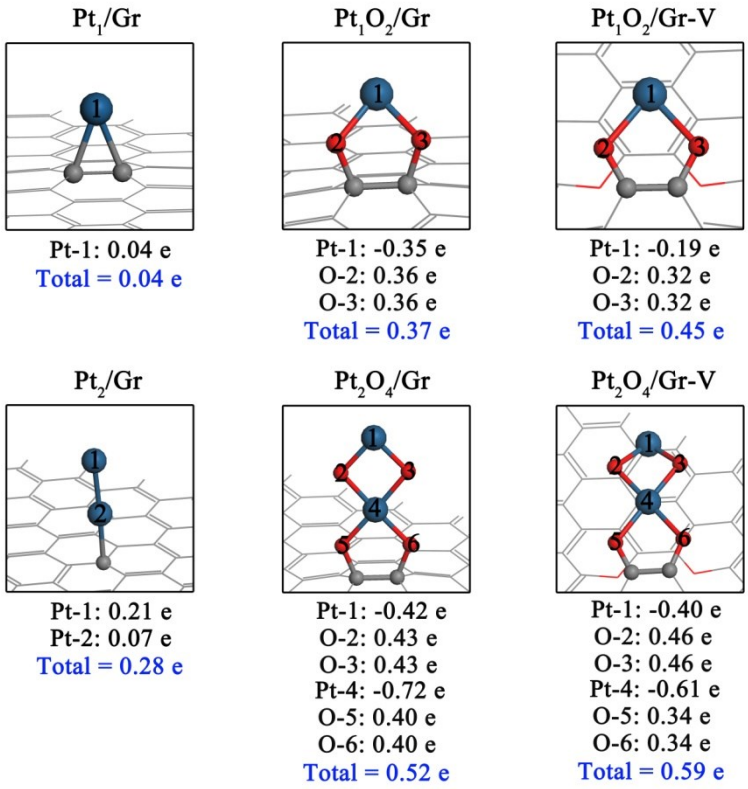

Figure S4. Binding structures and their corresponding DDEC charges of the Pt_1/Pt_2-tip on Pristine/Oxidized graphene. See Figure S1 for color coding.

6. The Optimized Structures and Binding Energies of the Adsorption States in Figure 2.

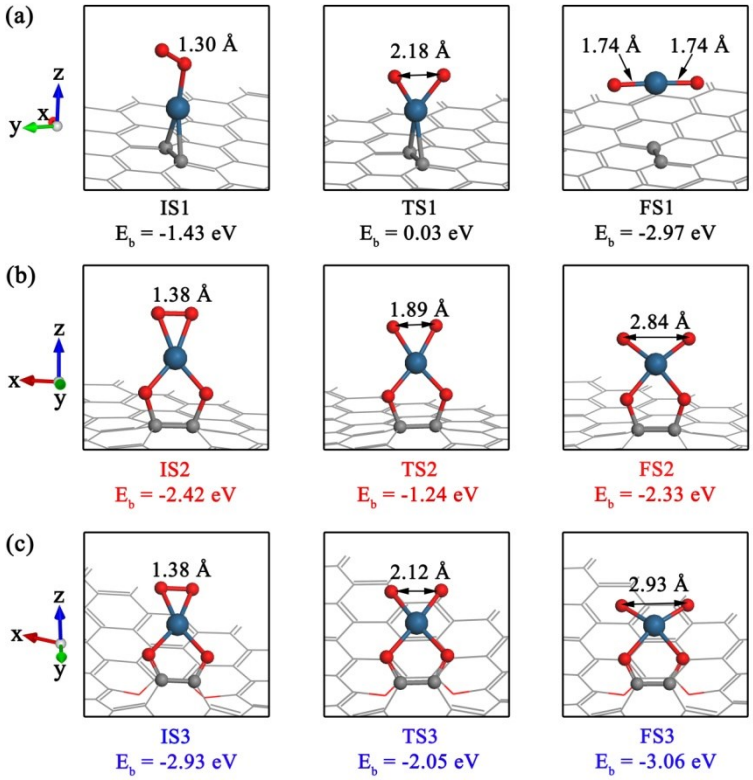

Figure S5. The optimized structures and binding energies of the adsorption states for the O_2 activation processes in Figure 2-(a). **(a)**, **(b)**, and **(c)** represent the states of O_2 on Pt_1/Gr, Pt_1O_2/Gr, and Pt_1O_2/Gr-V, respectively. See Figure S1 for color coding.

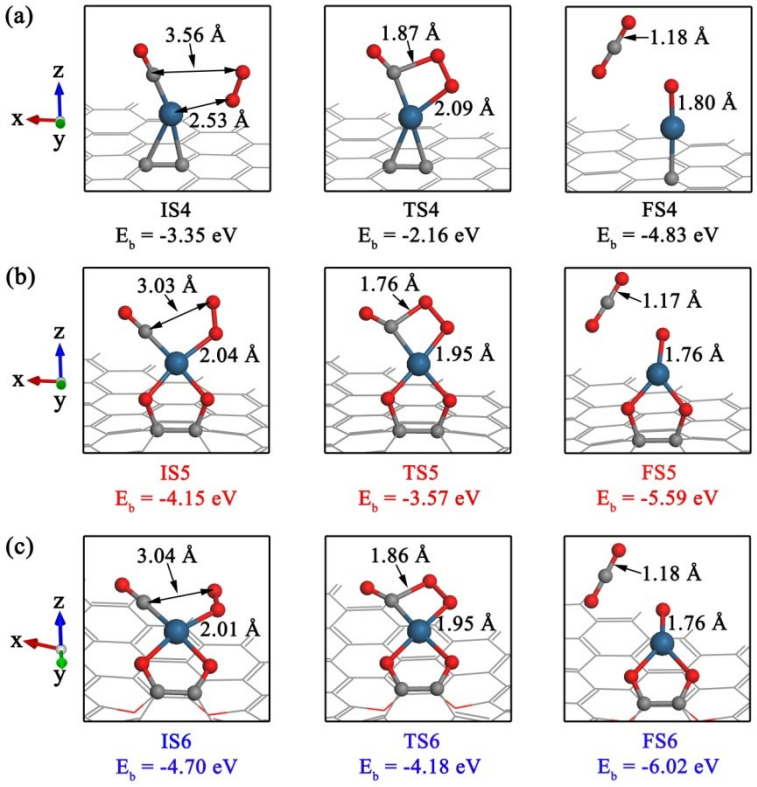

Figure S6. The optimized structures and binding energies of the adsorption states for the $CO+O_2$ processes in Figure 2-(b). **(a)**, **(b)**, and **(c)** represent the states of $CO+O_2$ on Pt_1/Gr, Pt_1O_2/Gr, and Pt_1O_2/Gr-V, respectively. See Figure S1 for color coding.

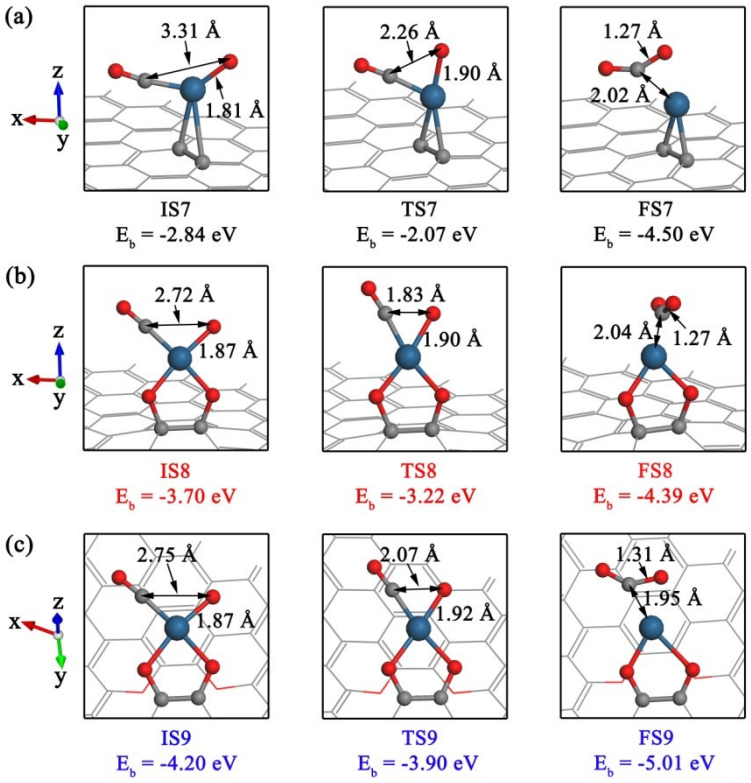

Figure S7. The optimized structures and binding energies of the adsorption states for the CO+O processes in Figure 2-(c). **(a)**, **(b)**, and **(c)** represent the states of CO+O on Pt_1/Gr, Pt_1O_2/Gr, and Pt_1O_2/Gr-V, respectively. See Figure S1 for color coding.

7. The Optimized Structures and Binding Energies of CO on the Pristine/Oxidized Graphene Supported Pt sites.

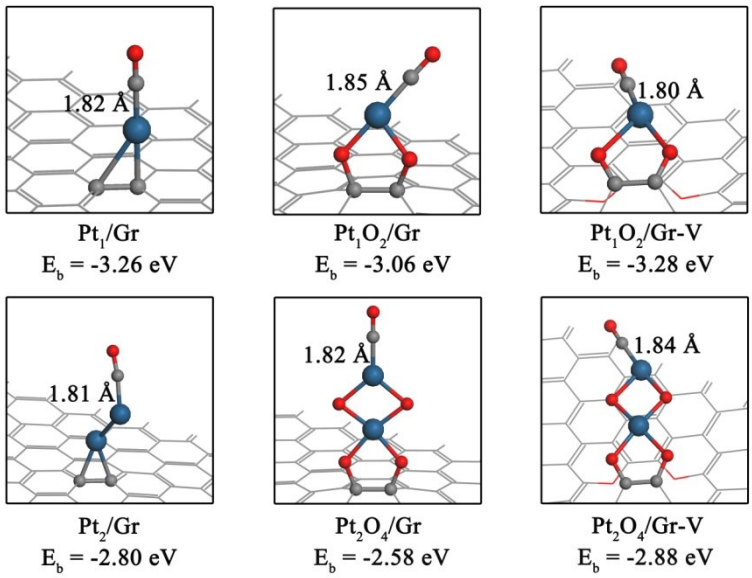

Figure S8. The optimized structures and binding energies of CO on the pristine/oxidized graphene supported Pt sites. See Figure S1 for color coding.

8. The Adsorption Trend of $2CO+O_2$ on Pt_1O_2/Gr.

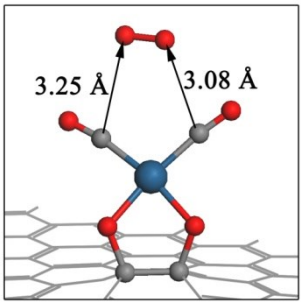

Figure S9. The adsorption trend of $2CO+O_2$ on Pt_1O_2/Gr. See Figure S1 for color coding.

9. The Optimized Structures and Relative Energies of the Pt_1O_2/Gr Catalysts with the Oxidized Ortho and Meta Carbon Vacancies.

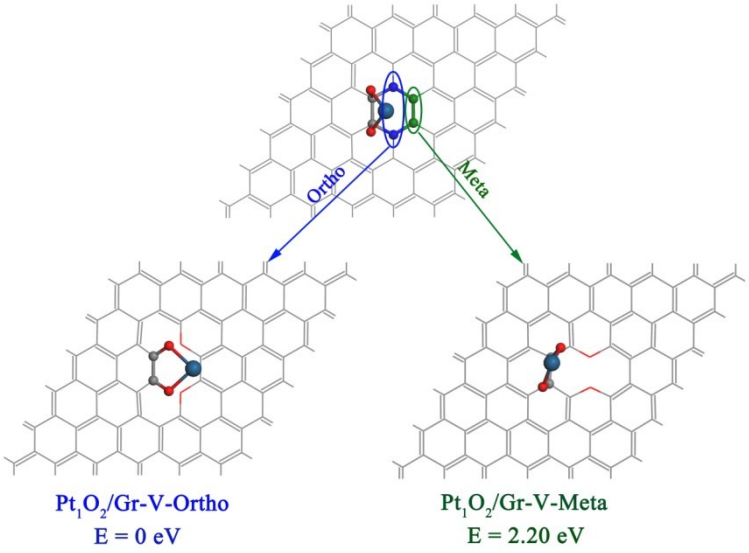

Figure S10. The optimized structures and relative energies of the Pt_1O_2/Gr catalysts with the oxidized Ortho and Meta carbon vacancies. Blue spheres: oxidized Ortho carbon vacancies; green spheres: oxidized Meta carbon vacancies; other atoms are the same as in Figure S1.

10. The Binding Structures of the Pt_2O_4 Cluster at the Ortho, Meta, and Para Positions of a Carbon Ring on Graphene.

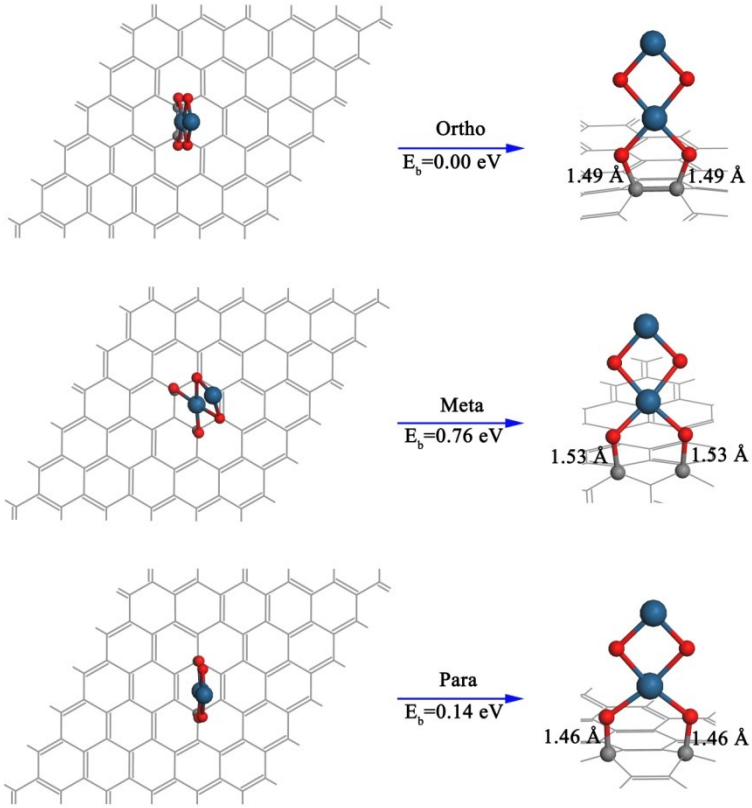

Figure S11. The binding structures and relative binding energies of the Pt_2O_4 cluster at the Ortho, Meta, and Para positions of the ring. Left: top-view; Right: side-view. See Figure S1 for color coding.

11. The Optimized Structures and Binding Energies of the Adsorption States in Figure 6.

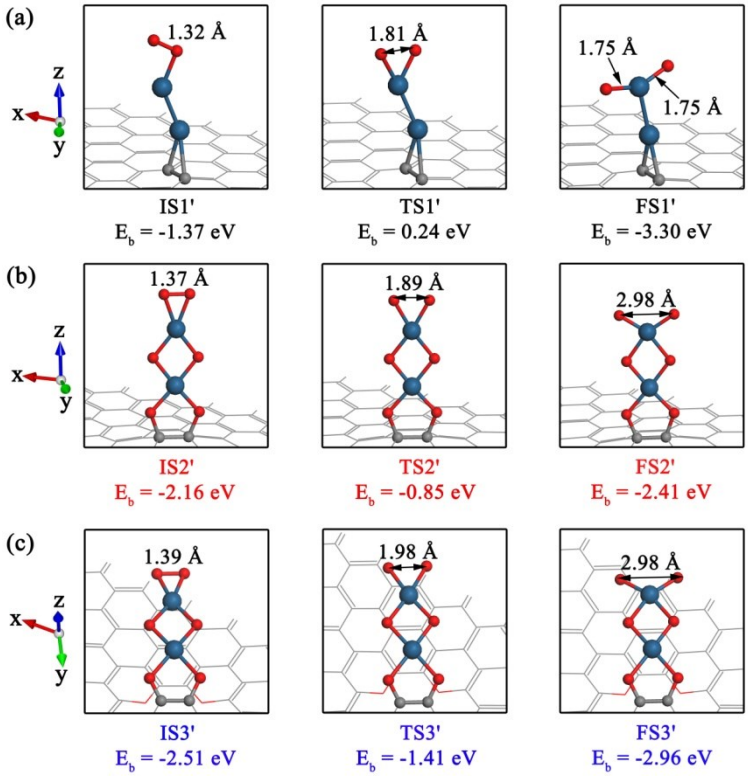

Figure S12. The optimized structures and binding energies of the adsorption states for the O_2 activation processes in Figure6-(a). **(a)**, **(b)**, and **(c)** represent the states of O_2 on Pt_2/Gr, Pt_2O_4/Gr, and Pt_2O_4/Gr-V, respectively. See Figure S1 for color coding.

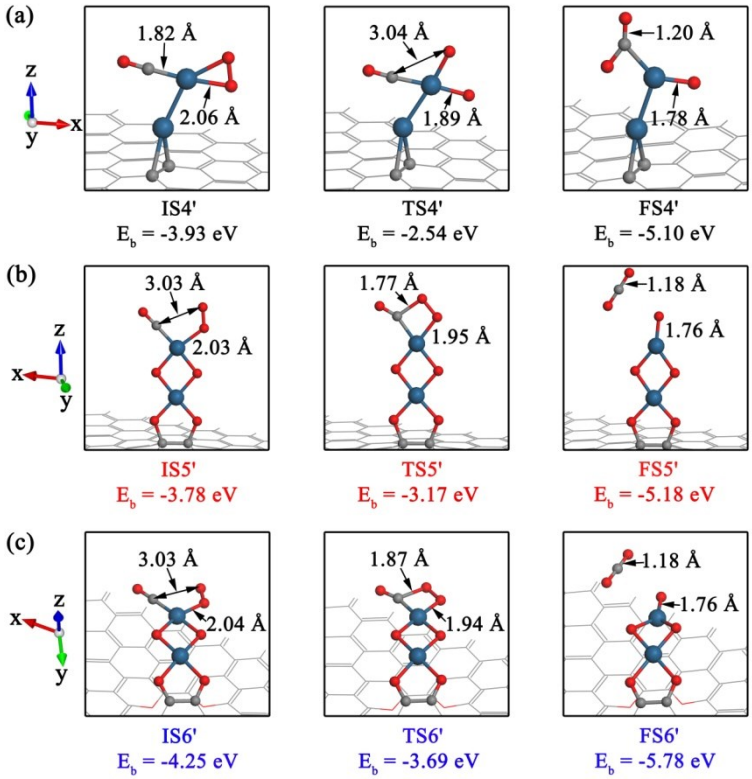

Figure S13. The optimized structures and binding energies of the adsorption states for the $CO+O_2$ processes in Figure 6-(b). **(a)**, **(b)**, and **(c)** represent the states of $CO+O_2$ on Pt_2/Gr, Pt_2O_4/Gr, and Pt_2O_4/Gr-V, respectively. See Figure S1 for color coding.

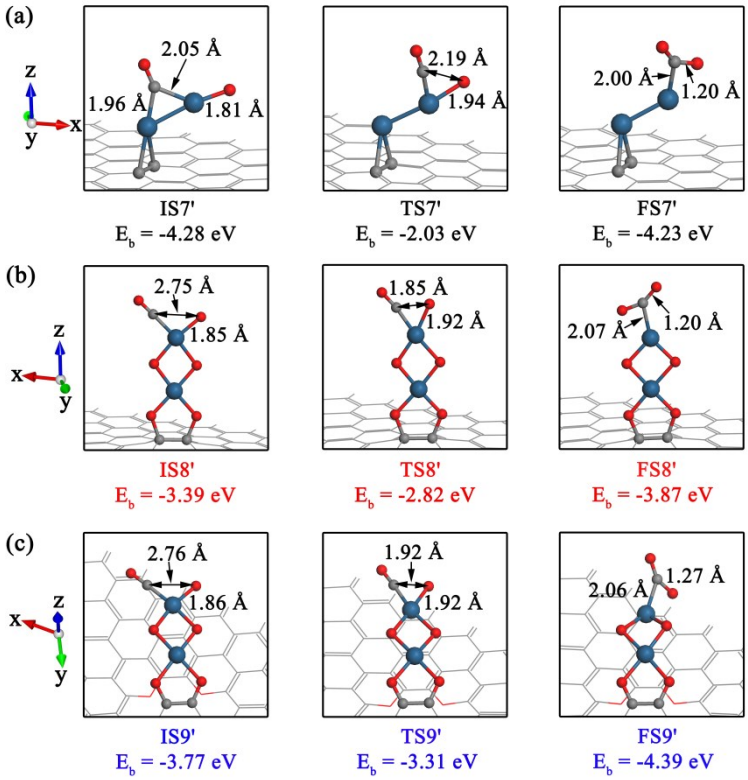

Figure S14. The optimized structures and binding energies of the adsorption states for the CO+O processes in Figure 6-(c). **(a)**, **(b)**, and **(c)** represent the states of CO+O on Pt_2/Gr, Pt_2O_4/Gr, and Pt_2O_4/Gr-V, respectively. See Figure S1 for color coding.

12. The Optimized Structures and Relative Energies of the Pt_2O_4/Gr Catalysts with the Oxidized Ortho and Meta Carbon Vacancies.

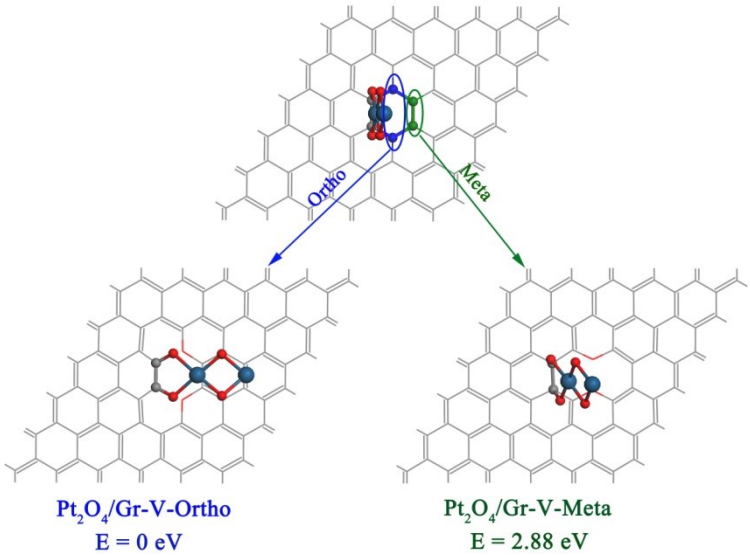

Figure S15. The optimized structures and relative energies of the Pt_2O_4/Gr catalysts with the oxidized Ortho and Meta carbon vacancies. See Figure S7 for color coding.

References

[s1] T. B. Rawal, D. Le and T. S. Rahman, *J. Phys. Chem. C*, 2017, **121**, 7282-7293.

[s2] X. Li, W. Zhong, P. Cui, J. Li and J. Jiang, *J. Phys. Chem. Lett.*, 2016, **7**, 1750−1755.

[s3] S. Sinthika, E. M. Kumar and R. Thapa, *J. Mater. Chem. A*, 2014, **2**, 12812-12820.

[s4] J. Zhao and Z. Chen, *J. Am. Chem. Soc.*, 2017, **139**, 12480-12487.